3D-circular surface curvature of spherule-based electrode for selective signaling and dynamic mobility of norepinephrine in living cells

M. Y. Emran,[1] M. A. Shenashen,[1] S. A. El-Safty[1,], M. M. Selim, [2] T. Minowa,[3] A. Elmarakbi,[4]*

[1] National Institute for Materials Science (NIMS), Research Center for Functional Materials, 1-2-1 Sengen, Tsukuba-shi, Ibaraki-ken 305-0047, Japan

[2] Department of Mathematics, Al-Aflaj College of Science and Human Studies, Prince Sattam Bin Abdulaziz University, Al-Aflaj, 710-11912, Saudi Arabia

[3] Nanotechnology Innovation Station, NIMS, 1-2-1 Sengen, Tsukuba 305-0047, Japan

[4]Department of Mechanical & Construction Engineering, Faculty of Engineering and Environment, Northumbria University, Newcastle upon Tyne, NE1 8ST, UK

** Corresponding author: sherif.elsafty@nims.go.jp*

KEYWORDS: Norepinephrine; Biosensor; Sulfur-doped carbon-based materials; Nanoporous carbon; Cytotoxicity and biocompatibility; Living cells

ABSTRACT: A highly sensitive protocol for signaling norepinephrine (NEP) in human fluids and neuronal cell line models should be established for clinical investigation of some neuronal diseases. A metal-free electrode catalyst was designed based on sulfur-doped carbon spheroidal surface (S-CSN) and employed as a transducing element for selective signaling of NEP in biological samples. The designed electrode of S-CSN features spherical construct and curvature surface to form spheroidal nanolayer with an average layer size of < 2 nm. The S-CSN shows surface topography of circular surface curvature with rugged surface texture, ridge end, and free open spaces between interlayers. The rich-space diversity surfaces offer forest electron transports and heavily target loads along with in-/out-plane circular spheres of the S-CSN surface. The active doping of the carbon-based electrode by S atoms creates an active transducing element with many active sites, strong binding to targeted molecules, facile diffusion of charges/molecules, long-term durability, and dense reactive exposure sites for signaling NEP at ultra-trace levels. S-CSN could be a sensitive and selective nanosensor for signaling NEP and establishing a sensing protocol with high stability and reproducibility. The sensory protocol based on S-CSN exhibits high sensitivity and selectivity with a low detection limit of 0.001 μM and a wide linear range of 0.01–0.8 μM. The in vitro sensory protocol of NEP secreted from living cells (neuronal cell line model) under stimulated agents possesses high sensitivity, low cytotoxicity, and high biocompatibility. These results confirm the successful establishment of NEP sensor in human blood samples and neuronal cells for clinical investigation.

1. Introduction

Norepinephrine (NEP), epinephrine (EPI), and dopamine (DA) are biogenic amines and regarded as monoamine neurotransmitters. Neurotransmitters play a significant role in various biological activities and function as signal transport elements in the brain and central nervous system.[1-4] The secretion of NEP from the adrenal gland usually increases under high-stress conditions, fighting, and any dangerous situation. This secretion increases the blood flow for muscles and brain as oxygen and glucose production support.[5-8] Moreover, NEP is used in treatment of diseases, such as hypertension, heart disease, diabetes, and anxiety.[1, 5, 7] The fluctuation of NEP levels acts as a biomarker for neurological diseases, such as schizophrenia, Parkinson's disease-, and Alzheimer's disease.[9-11] In this regard, scholars have focused on establishing a highly sensitive protocol with long-term stability, on-site measurement, and high economic value for detection of NEP in human blood samples, brain slices, and living cells for clinical and neurological applications.

Controlled detection of NEP can be conducted using various analytical techniques, such as high-performance liquid chromatography, [12] fluorescence microscopy, [13,14], and electrochemistry. [3, 15, 16] Most of these techniques are sensitive and selective but require sophisticated procedures, time-consuming process due to sampling preparation, highly expensive machines, and highly trained technician. Electrochemical techniques exhibit high sensitivity and selectivity, easy to use, and fast response and are suitable for in vivo and in vitro applications.[16-18] Thus, electrochemical NEP sensor/biosensor is widely used given its high selectivity in the presence of other interfering molecules.[3, 15, 16, 19] Several approaches based on the design of modified electrodes have been established for detection of NEP; these electrodes include functionalized MWCNTs with electrodeposited luteolin, poly trypan blue modified GCE, 5-amino-3′,4′-dimethyl-biphenyl-2-ol (5ADB), and ZnO/CNTs.[15,19-21] The ITO-electrode modified with CN@NiO with novel broccoli-

shaped NiO was used for selective signaling of NEP in living cells. The designed electrode showed high sensitivity, good selectivity in the presence of potentially interfering species, high stability, and reproducibility.[3]

The simple and controlled synthesis and construction of carbon-based materials as sensors and biosensor-based electrodes have attained a great interest. [4, 8, 22-24] Various types of carbon-based materials have been used as working materials due to their good electrochemical properties, easy fabrication, and facile functionality; such materials include graphene, carbon nanotubes, fullerenes, diamond, carbon nanomaterials and their composites.[4, 8, 24-28] Significant properties of large surface area, good mechanical stability, good conductivity, easy fabrication and functionalization, and composite formation within the metal and/or metal oxides have gained particular interest in various fields, such as biosensing, water treatment, and energy.[28-36] Several approaches have been reported for enhancing the activity of carbon-based materials by doping the carbon chain by non-metal heteroatoms, such as boron (B), phosphorous (P), nitrogen (N), and sulfur (S).[4, 8, 22, 37-40] Doping of S atoms in the carbon chain enhances the electrochemical activity. The mechanism of action remains unclear because the electronegativity of S (2.58) is close to C (2.55). Thus, the action of S atoms to the activity of carbon materials may be related to increased electron spin density and outer surface functionalization by sulfur groups.[41,42] The active interfacial surface based on the S-doped carbon offers a highly electrochemical surface with functionalized active sites, high molecular loading, and fast charge transport.[41,42] Therefore, the function of chemical components of S-doped carbon-based materials and surface topography of curvature, meso-grooves, vortices, ridge end, rugged surface, and nanoplates play key roles for establishing a highly sensitive sensory protocol for NEP detection.

Herein, spheroidal S-doped carbon-based materials were synthesized and employed for sensitive and selective signaling of NEP in human blood serum and a neuronal cell line model. S-CSN acts as a signaling transduction element of the electro-oxidation process on the electrode surface and exhibits fast response, low charge resistance, and numerous active centers. S-CSN has a spheroidal morphology with stocked nanolayers, rough surface texture, bundle surface meshes, ridge end with 3D orientation, S-doped graphitic carbon, and microporous network. Furthermore, the surface topography of meso-grooves, voids, protuberances, and interfaces running over the outer surface of electrodes is woven into tightly folded sensor surfaces. Therefore, S-CSN ascertains a highly active interfacial surface for facile diffusion of targeted molecules. NEP strongly binds to the S-CNS-surface and is oxidized with an active signaling transaction through a sensitive, selective, facile, stable, and reproducible protocol. Real monitoring of NEP in various sources, such as human blood serum and living cells (acted as a neuronal cell model), was conducted using the S-CNS-modified electrode (Scheme 1). The designed S-CNS-based nanosensor showed high sensitivity, good selectivity, high stability, durable reproducibility, low cytotoxicity, and high biocompatibility for in vitro detection of NEP.

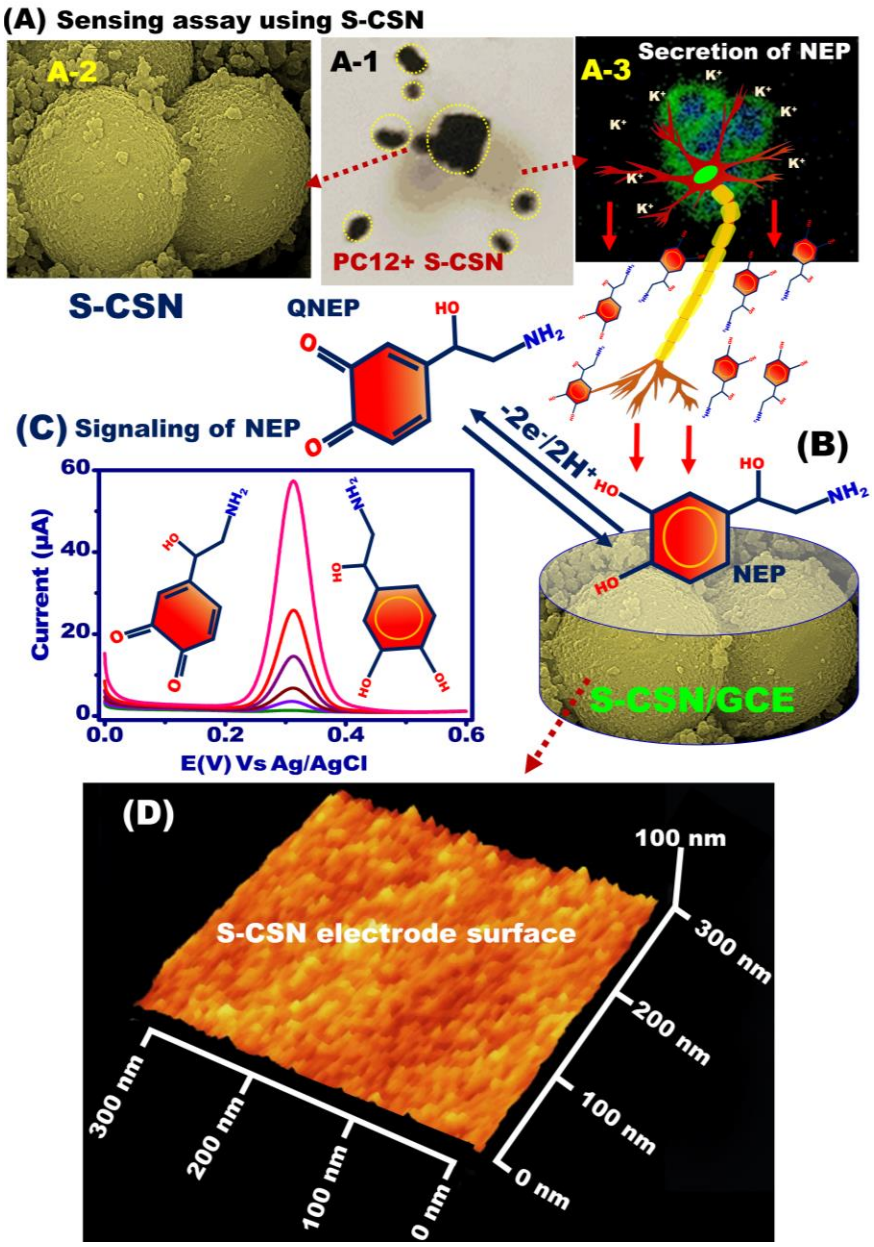

Scheme 1. Design of sensing assay based on S-CNS was approached for detection of NEP secreted from living cells. A-2) S-CSN geometric structure of 3D-circular surface curvature of spherules. A-1) Incubation of S-CSN with neuronal cell line model (PC12). A-3) The PC12 synthesis NEP, and the liberated NEP increases as increasing the KCl-concentration (stimulated agent). B&C) The NEP-sensor based on S-CNS/GCE transduces the electrooxidation signal of NEP using SWV-measurements. D) The atomic force microscopy (AFM)-image of S-CSN.

2. Experimental section

2.1 Electrode synthesis and fabrication of 3D circular S-doped carbon spheroidal surfaces of S-CSN

2.1.1 Synthesized of 3D circular S-doped carbon spheroidal surfaces

Controlled formation of S-doped carbon-dense spherical aligned nanolayer (S-CSN) was conducted based on a simple hydrothermal treatment (HT) of hydrocarbons such as glucose and thiourea in the presence of capping agent F127.[8, 24] The synthesis procedure and condition were controlled as follows. Thiourea, α-D-glucose, Pluronic F-127, and distilled H_2O were mixed with the following ratios 0.25:1:1:32.5 and 0.5:1:1:32.5. The solutions were sonicated for 1 h and stirred for 2 h. Samples 1 and 2 were transferred into 100 mL Teflon-lined autoclaves and supported at 180 °C for 24 h. After cooling, a black precipitate of S-CSNs was formed. The S-CSN materials were washed many times by water/ethanol and dried at 60 °C for 24 h. For complete carbonization, the S-CSN materials were calcined at 800 °C under N_2 flow for 4 h with a step temperature increase of 5°C/min and named as S-CSN-1 and S-CSN-2.

2.2 Fabrication of 3D circular S-doped carbon spheroidal surfaces (S-CSN) as working materials

The electrode fabrication for sensing of NEP was assigned as follows: a) the material ink formation was prepared by diffusing 5 mg of S-CSN-1 and S-CSN-2 in 1 mL dis.H_2O and further used for electrode modifications. b) The glassy carbon electrode cleaning (GCE): The GCE (diameter 3.0 mm) was cleaned by polishing the electrode surface to be like a mirror using 0.05 μM alumina slurry, then polished in diamond slurry. At every step the electrodes were washed by dis.H_2O every sweep. After that, the electrode was sonicated in acetone and dis.H_2O solution for 30 min. c) The multidimensional surface electrode of S-CSN was designed by formation of a thin layer at the

GCE-surface based on drop-casting of 20 µL of S-CSN-1, and S-CSN-2, then keep drying at room temperature. d) The designed electrode activation; the working electrodes were activated using continuous cyclic voltammetry sweeps for 10 cycles within the potential window of 0.0 - 1.8 V in 0.1 M PBS (pH = 7) at a scan rate of 100 mVs^{-1}.

2.3 Cytotoxicity

The cytotoxicity of S-CSN-1 on the PC12 cells was investigated using Cell Counting Kit-8 (CCK-8) assay. The PC12 cells (5×10^5 cells/mL) were moved onto 96-well microplates and kept in the incubator at 37 °C under a 5% CO_2/95% air for 24 h. Then, various concentrations of S-CSN-1 were added (10 mL of 10, 20, 50, 100 and 200 µg/ml), and incubated for 48 h. The CCK-8 solution (10 µL, 5 mg/mL) was added to each well, then incubated for 2-4 h. After that, the incubated cells were measured using a microplate reader at an absorbance of 450 nm.

2.4 Cell culture and in vitro study

Cell culture growth and passaging of PC12 cells. The cells of PC12 were passaged every 6-days and kept in the incubator under 5% CO_2 at 37 °C. The medium was changed two-times a week throughout the lifetime of all cultures. The medium was prepared as follow: a 50 mL fetal bovine serum (FBS), and 50 mL heat-inactivated serum were added to 500 mL of Dulbecco's Modified Eagle's Medium (DMEM).

For PC12 cells visualization experiments using S-CSN-1; the 5×10^5 cells/mL of PC12 cells were sowed in 6 well-plate for 24 h and kept in the incubator. The cells were stained by phalloidin 488(1/500 mL) in PBS for the F-actin staining, and were stained by 4', 6-diamidino-2-phenylindole (DAPI) (1/1000 mL) in PBS for nuclear counter-staining for 5 min. Finally, the PC12 cell's images were captured at ambient temperature using a confocal laser scanning microscopy (Leica TCS SPE5 X). PC12 cells were incubated with 20 µL of various concentrations of KCl (0–50 mM) to

study the effect of K^+-ions on the amount of NEP secreted. The solution was incubated in a humid chamber under 5% CO_2 at 37 °C for 30 min and centrifuged. The supernatant was used to evaluate the liberation of NEP form PC12 cells.

3. Results and discussion

3.1 3D circular curvature surface design of S-doped CSN for selective monitoring of NEP

Scheme 1 shows the effective synthesis of the 3D-circular surface electrode based on S-CSN. The building of 3D circular surface of S-doped carbon-based electrode ascertains the modulation of highly active interfacial surfaces. The active surface modulation of multiple architectures, geometries, and a mixture of various heterogeneous constructs led to the formation of high loading and wide interactive surface. The variable geometries of 3D circular surface of S-CSN-based electrode conjugated with meso-grooves, jugged texture, and ridge end was designed. S-CSN generated a highly sensitive and selective nanosensor for screening of NEP with powerful molecular diffusion throughout out-/in- then up-/down-ward entrances and multiple discharge rates. Therefore, the geometry and chemical composition of S-CSN could be utilized to design a selective sensor for on-time sensing of NEP secreted from the neuronal cell line model.

3.2 Controlled formation of 3D circular S-doped carbon spheroidal surfaces

The controlled synthesis of 3D circular -CSNs was conducted using hydrothermal treatment (HT). The HT of carbohydrates led to the formation of carbon materials based on successive condensation, polymerization, and aromatization.[43] Active doping of carbon materials with heteroatoms of S was conducted through one-pot method of carbon source (glucose) and S atom source (thiourea) at an elevated temperature of 180 ºC for a long time of 24 h. The thiourea acted as the S-atom sources and shared the structural formation of the desired carbon material. Scheme

2 shows the controlled formation of porous carbon materials. The 3D circular shape formation similar to a stocked layer formation was obtained by adding the capping agent F127 as a soft template and as a directing agent. After calcination at 900 ºC, F127 was removed and a porous carbon material was formed with a new spherical morphology (spheroidal structure). Various concentrations of thiourea were added to obtain two samples, namely, S-CSN-1, and S-CSN-2. For complete carbonization, the desired materials were annealed at 900 °C under N_2 flow at a raising temperature rate of 5 °C/min. The materials were placed in a desiccator until further use and labeled as S-CSN-1 and S-CSN-2.

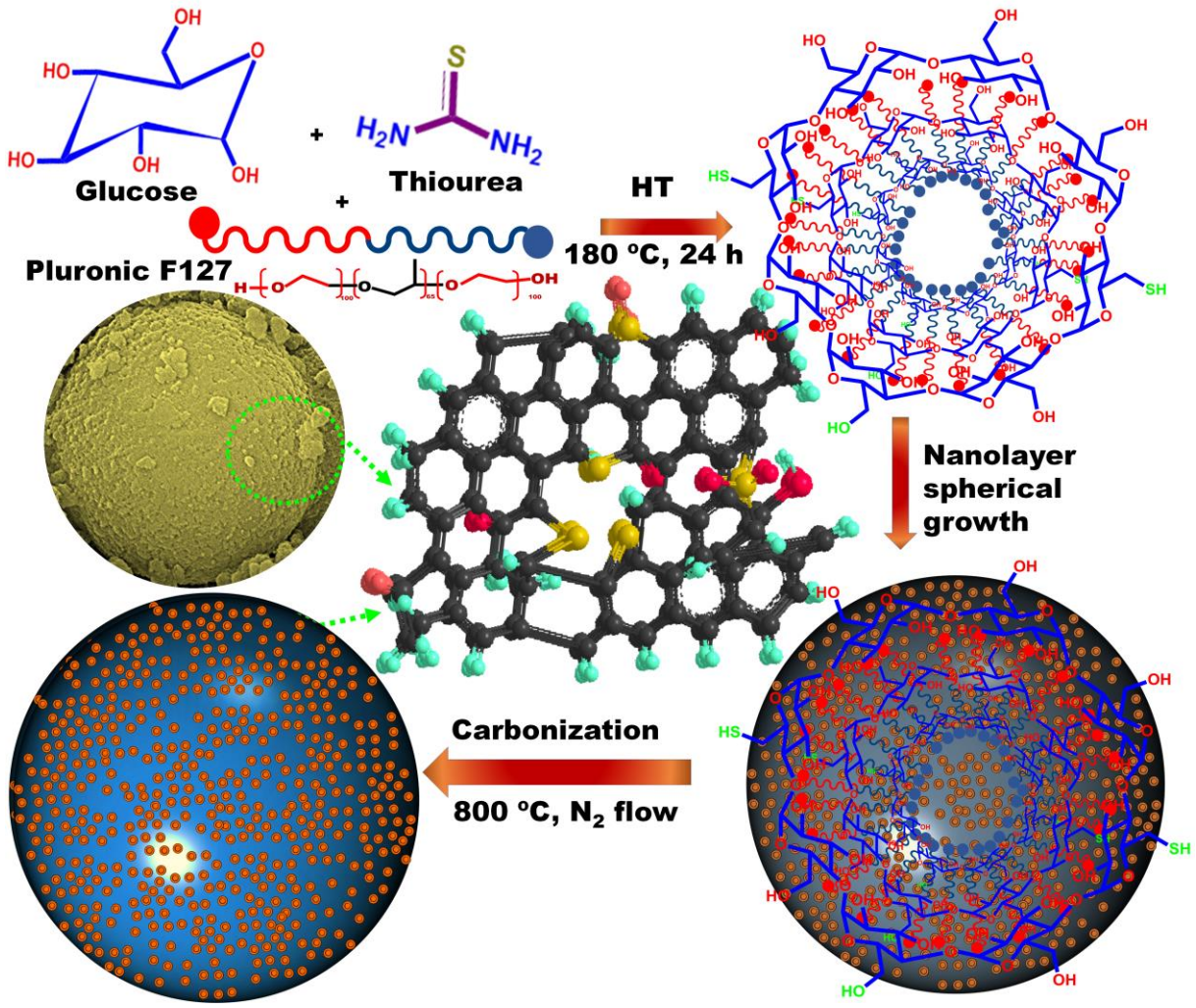

Scheme 2: Schematic formation of the S-CSN within starting materials of glucose as carbon source, thiourea as S atoms source, and F127 as a directing agent. Within variation of the thiourea concentrations, two various materials were synthesized and named as S-CSN-1, and S-CSN-2.

The surface morphology of the prepared materials of 3D circular S-doped carbon spheroidal surfaces was investigated using field-emission scanning electron microscopy (FE-SEM) (Figure 1). Figure 1A shows the spherical morphology of S-CSN-2 with a stocked layer of S-doped carbon-based materials. The rough surface and the small particles around the spheres form a layer-by-layer structure as the action of F127 (Figure A-a). The 3D orientation and shape of S-CSN with a dense nanolayer of spherule structure were formed. Figure 1(A-b&A-c) shows the high focusing

SEM image at various positions and cross-sections of top-view (b) and side view (c) to confirm the formation of spheroidal surfaces with curvature structure and 3D orientation. The spheres are rough with ridge ends, confirming the predicted mechanism of the formation of spheroidal layer by layer similar to the deposition of layer-by-layer along one axis. The layer size range is too small (1–2 nm). The S-CSN-1 spherical construct is small and quite distorted to form a 3D circular orientation and formation of spheroids. The spheroidal formation like a rotation of layer-by-layer to form an ellipse around an axis (Figure 1B-a). The presence of F127 thiourea through the carbonization leads to the formation of curvature surface with dense spherical nanolayers. Figure 1(B-b& B-c) obtains the spheroidal stocked layer formation as the spherical growth of layer by layer construction with open spaces between layers. S-CSN-1 is formed by carbon layer deposition around one axis to form a spherical construct of carbon-based materials with open hole-like cavity with micor-/nano-/macro-pores and grooves. The surface texture is rough with a 3D curvature structure and ridges (Figure 1B-c). Focusing on the top-view of the formed spheroidal surface shows a fraction of layers formed with nano-grooves inside. The size of the layer ranges from 2 nm to 5 nm, and the full sphere size is 0.5 μm (Figure 1B-b). The atomic distribution of C, O, and S atoms on the surface of S-CSNs to obtain efficient carbonization was investigated using EDX-SEM. Figure 1(C-a–C-c) shows the EDX-SEM mapping of S-CSN-2 for C, O, and S atomic distribution. The homogeneous distributions of C, O, and S atoms on the surface of S-CSN-2 with 63.17% C, 31.96% O, and 4.87% S are presented. The atomic contents and homogeneous distribution of C, O, and S of S-CNS-1 were observed with various contents of %C (71.36), %O (25.58), and %S (3.06) (Figure S1[A-a–A-c]). The C and S contents in S-CSN-1 to S-CSN-2 vary and may influence the electrochemical activity.

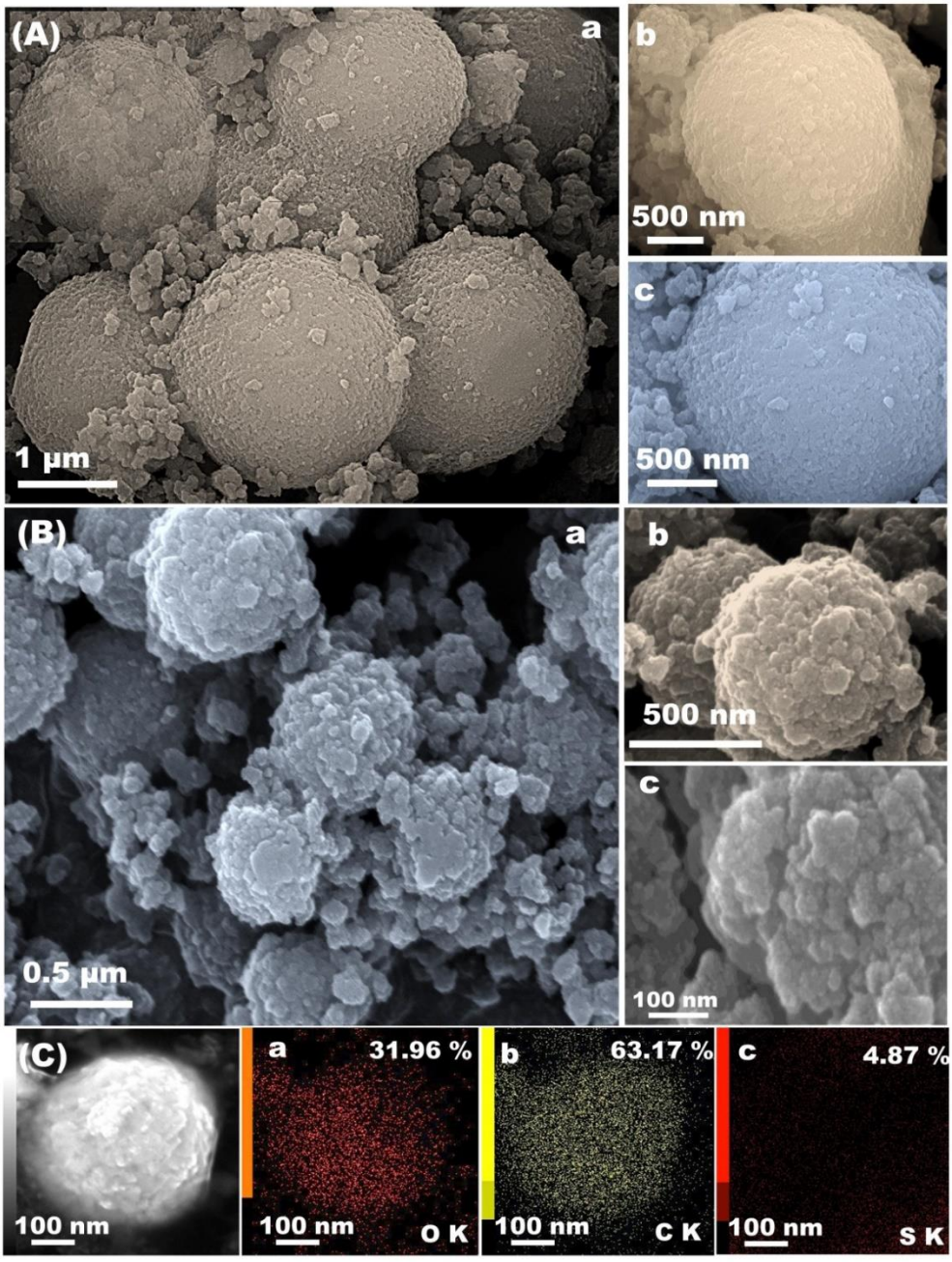

Figure 1. A) FE-SEM-images of the S-CSN-2 with low magnification (a). b&c) High focusing FE-SEM-images on outer surface topography of S-CSN-2. B) The FE-SEM-image of S-CSN-1 at low magnification (a). b&c) High FE-SEM magnification, focusing on the surface texture and obtaining stocked layer-by -layer formation of 3D-circular surface curvature of S-CNS-1. C) EDX-SEM mapping of S-CSN-2 of C (a), C (b), and S (c).

Dark (DR)- and bright field (BF)-, scanning transmission electron microscopy (DF- and BF-STEM) were employed to confirm the ridged ends and curvature of the 3D spheroidal structure of S-CNS-1 (Figure 1[A-a–A-c]). Figure 1A-a& A-b confirms the spheroidal growth of nanolayers with ultrathin size and 3D -orientation of S-CSN-1. The bright-field (BF)-STEM confirms the spheroidal formation with rough surface texture, 3D curvature orientation, and weaved surface. The dense nanolayer, ridge ends, and U-undulation are presented in Figure 1A-c. Therefore, The S-CNS surface of the heterogeneous surface of ridge ends, rough surface texture, 3D curvature orientation was successfully designed for potential sensing and biosensing application. Figure 2B-a shows the HRTEM of S-CSN-2 and reveals the spheroidal surface with nano-porous construct and curvature surfaces. The surface ends are rough with ridged ends (Figure 2B-b). The spherical growth is similar to the deposition of a nanolayer around one axis to form spheroidal constructs and confirms the heterogeneous surface with ridge end, curvature, and rough surface.

The formation of porous carbon materials and the surface area of S-CNS-1 and S-CNS-2 were evaluated using N_2 adsorption isotherm. Figure 2C shows the N_2-adsorption isotherm of S-CNS-1 (violet line) and S-CNS-2 (green line). The N_2 adsorption behavior displays a typical type I isotherm, in which a sharp uptake at low P/P_0 ($P/P_0 = 0.02$) and high uptake at a high relative pressure ($P/P_0 > 0.9$) were observed. This behavior is related to the microporous network formation.[44-47] Figure 2D shows the NLDFT-pore distribution of S-CNS-1 (violet line) and S-CNS-2 (green line), confirming the N_2-adsorption data for the presence of microporous particles with pore size ranging from 1.5 nm to 2.2 nm. The surface areas (S_{BET}) of S-CNS-1 and S-CNS-2 are 612 and 164 m^2g^{-1}, respectively. These results illustrate the large surface area and microporous morphology of S-CNS-1. The 3D circular S-doped carbon spheroidal surface formation and the effect of S atoms on the graphitic nature were determined using Raman shift microscopy. Figure

S1B shows two Raman shift peaks of S-CSN-1 (violet line) and S-CSN-2 (green line), centered at 1350 and 1560 cm^{-1} for G and D bands, respectively. The presence of G band refers to the presence of sp^2 hybridization (graphitic construction chain formation), while the D band refers to the distortion of the graphitic construct (sp^3-hybridization). The presence of S and O atoms in the graphitic carbon chain are indicated by the presence of D band and refers to the distortion of the sp^2 hybridization. The I_D/I_G values of 0.89 and 0.94 for S-CSN-1 and S-CSN-2 confirm the degree of graphitic nature and distortion order.[48,49] These results confirm the successful doping of S-atoms in the carbon-based material. In addition, the low I_D/I_G ratio for S-CNS-1 is related to the decrease in the O content, high carbon content, and the effect of S dopant. The carbonization conformations of S-CNS-1 and S-CNS-2 were investigated using WA-XRD. Figure S1C shows two WA-XRD broad peaks centered at $2\Theta = 29.65°$ and 42° for S-doped carbon materials. These peaks are related to the amorphous graphitic carbon formation. The presence of a peak at $2\Theta = 42°$ indicates the distortion of the graphitic construct and supports the presence of heteroatoms, such as O and S, through the graphitic chain. The XPS analysis shows three peaks at around 166, 284.28, and 527 eV for S 2p, C 1s, and O 1s, indicating the chemical components of S-CNS (Figure S1D). The XPS spectra of S 2p (Figure S1F), C 1s (Figure S1E), and O 1s (Figure S1G) show the formation of carbon materials with active doping of S atoms (for additional details, see Supporting Information). The presence of C-SO_2-C, and C-S-C were confirmed by XPS-analysis of S 2p. Therefore, the active electrode surface of S-CNS displays strong binding and facile diffusion of NEP molecules as the presence of SO_X group at the outer surface. The designed nanosensor based on S-CNS has abundant active centers, microporous network, S incorporated to the carbon chain, rough surface texture, 3D spheroidal orientation, meso-grooves, and open networks, forming a highly interfacial electrode surface. The electrode surface topography and thickness were shown

by using AFM analysis (Scheme 1D). The AFM microscopic patterns showed that the fabricated S-CNS surface has a degree of roughness with multiple vacancies. The topographic image with rough and heterogeneous arrangements along the electrode surfaces indicates for multi-functional diffusion of NEP analytics.

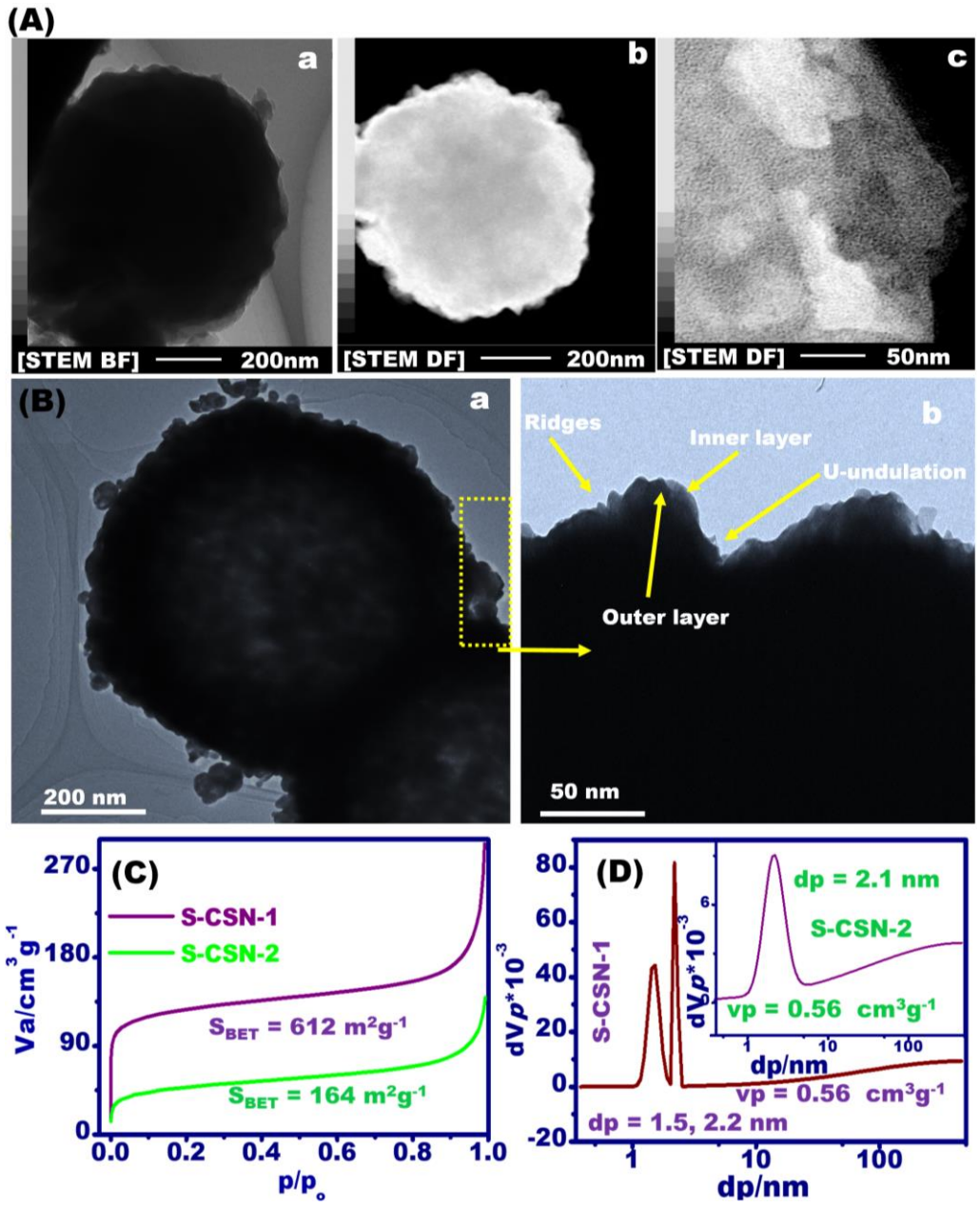

Figure 2. A) BF (a)- and DF-STEM images of S-CNS-1 (b&c). B) HRTEM images of S-CNS-2 with focusing on the spherule formation morphology (a) and focusing on the outer surface

topography (b). C) The N_2 adsorption isotherm of S-CSN-1 (violet line), and S-CSN-2 (green line). D) The NLDFT pore size distribution of S-CSN-1 (violet line), and S-CSN-2 (green line).

3.3 Catalytic activity and sensing property of S-CNSs

The catalytic activity of S-CNS-1- and S-CNS-2-modified electrodes and bare GCE was determined in $[Fe(CN)_6]^{3-}$ solution by using cyclic voltammogram (CV) (Figure S2A). The S-CNS-1-modified electrode (Ia = 24.28 μA) obtains the highest catalytic activity and fastest charge transfer compared with the S-CNS-2-modified electrode (Ia = 16.02 μA) and bare GCE (Ia = 12.64 μA). This finding may refer to the effects of the topography, morphology, and chemical components of the designed electrode with rough curvature surface, high surface area, microporous construction, and efficient S content. In addition, the active catalytic surface areas are 0.005, 0.006, and 0.009 cm^2 for GCE, S-CNS-2-, and S-CNS-1-modified electrodes, respectively, as determined by applying the Randles–Sevick formula [for more details, see supporting information, Figure S2A].[50] These data support the high electrode surface area and the significant increase in the sensitivity and catalytic activity of the modified electrodes.

The surface charge transfer and electron diffusion activity of the modified electrode was further confirmed. Impedance microscopy (EIS) was conducted on S-CNS-2- and S-CNS-1-modified electrodes in 0.1 M PBS (pH =7) holding 0.001 M $[Fe(CN)_6]^{3-}$ (Figure S2B). [51-52] The S-CSN-1-modified electrode shows the lowest semicircle and high diffusion line pathway compared with the S-CSN-2-modified electrode and GCE [for additional details, see supporting information, Figure S2B]. The S-CSN-1-modified electrode exhibits the lowest surface charge resistance and high electron diffusion. Figure S2C shows Zeta potential plot of S-CNS-1 in various pH values. The finding indicates that the overall charge onto the S-CSN-1 electrode surface is a negative

charge at pH 6.0-8.0 range. Therefore, the negatively charged surfaces enhance the binding events with NEB molecules, leading to high sensitivity and selectivity of the electrode. Thus, S-CSN-1 electrode provides good electrochemical activity in terms of fast charge transport, high electron diffusion, negative surface charge, and low charge distance pathway.

The sensing property of S-CNS-1- and S-CNS-2-modified electrodes and bare GCE for sensitive and selective signaling of NEP was determined using CV. The CV measurements illustrate the electrochemical oxidation-reduction peaks of NEP using various electrodes. As presented in Figure S2D, the oxidation–reduction peaks of 20 μM NEP were obtained for S-CNS-1- (violet line), S-CNS-2 (green line)-modified electrodes, and GCE (black line). Various anodic and cathodic current values and applied potential peak positions were observed as the electrode changed. The S-CNS-1-modified electrode displays higher NEP sensing property at low applied potential compared with the S-CNS-2-modified electrodes and GCE. The current values (Ia) of the anodic peaks are 33.29, 17.87, and 12.16 μA that recorded at applied potentials of 0.30, 0.33, and 0.494 V for S-CNS-1, S-CNS-2 and GCE, respectively. The S-CNS-1-modified electrode provides high sensitivity for signaling NEP at a low applied potential. These results may relate to a) the high surface area, b) porous construction, c) morphology of the spherical monolayer with open spaces in between, d) rough surface, and e) efficient S content. [3-4, 8, 24] CV measurements were conducted with and without 20 μM NEP to confirm the active signaling of the S-CSN-1-modified electrode (Figure S2E). The redox peaks were observed with high catalytic current value and may be related to the oxidation–reduction of NEP with high sensitivity. Scheme 3 illustrates the design of sensitive NEP biosensor based on the S-CNS-modified electrode and presents the facile diffusion and binding through the porous network and activity centers. The liberated NEP form neuronal cell line was detected. As a result of the effect of stimulating agents, the increase in the

level of neurotransmitters in living cells is distinct. These results indicate that the S-CSN-1-modified electrode can be employed for sensitive signaling of NEP in various human samples for clinical applications.

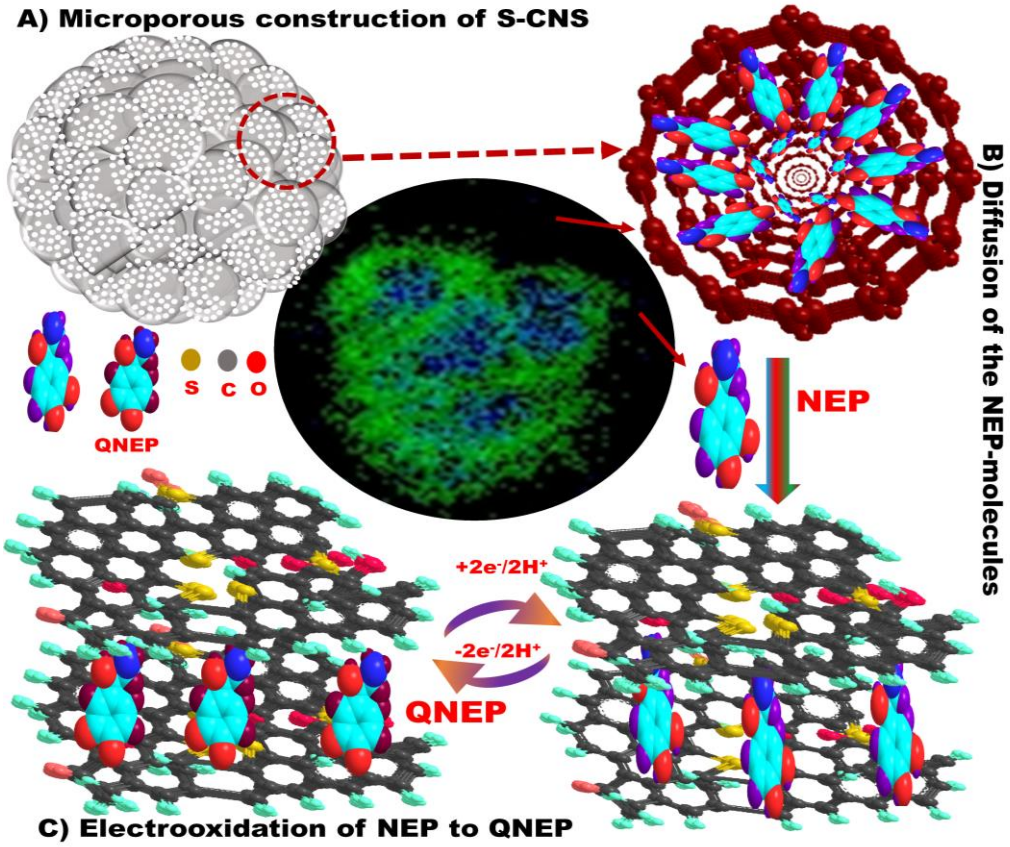

Scheme 3. A) Porous construction of S-CSN-1 with micro-, and meso-pores distribution. B) Diffusion and binding of the NEP-molecules through the inner/outer surface for facile sensitive and selective sensor. The S-CSN-1 acts as the transducing elements for highly sensitive detection of NEP. C) At the electrode surface of S-CSN-1, the oxidation-reduction of NEP to QNEP and the reverse process with losing and accepting of $2e^-/2H^+$ was proceeded with fast charge transport, and low surface resistance.

3.4 Electrochemical set conditions of NEP on S-CSN-1-modified electrode

The CV profile was obtained at a scan rate of 100 mV/s in 0.1 M PBS with pH range of 5-8 to study the effect of electrolyte pH on NEP oxidation–reduction. Figure 3A demonstrates the effect of electrolyte pH on the current peaks of the anode oxidation and cathode reduction of NEP target. The optimum pH–catalytic current value was found at pH = 7, which is similar to the pH of human physiological fluids. Figure 3B (green scatter) shows the scattering plot of pH versus the anodic peak current. The fluctuation in the current value indicates the significant effect of pH. The applied potential position E(V) shifted to negative values with increasing pH. The negative shift in the potential suggests the key effect of H^+ ions on the oxidation–reduction process of NEP on the S-CSN-1-modified electrode. The pH versus E(V) potential function shows a linear relationship according to the following equation of E(V)= 0.7 – 0.054 pH, R^2 = 0.99 (Figure 3B [violet scattering]). The slope value is 54 mV, which is in agreement to the Nernst theoretical value of 59 mV. This finding suggests that the NEP redox mechanism follows $2e^-/2H^+$. [3, 53-55]

The surface interaction property of NEP on the S-CSN-1-modified electrode was illustrated using the performance of the NEP at varying scan rates. Figure 3C shows the CV measurements of 20 µM NEP at varying scan rates of 10–300 mVs^{-1} on the S-CSN-1-modified electrode. The anodic and cathodic current values increase with increasing scan rate from 10 mVs^{-1} to 300 mVs^{-1}. By plotting the scan rate (mVs^{-1}) versus the anodic current (Ia) and cathodic current (Ic) (µA), linear relationships were obtained for both Ia and Ic, with the following equations: Ia (µA) = 8.12 + 0.3 ν (mVs^{-1}), R^2 = 0.993(S/N = 3); and Ic (µA) = -2.56 - 0.119 ν (mVs^{-1}), R^2 = 0.997 (S/N = 3) (Figure 3D). Thus, the overall surface interaction process is adsorption controlled. [4, 8, 56-57] Moreover, the surface components of S-CNS were composed of C-, S-, and O- atoms and formulated the following C-S-C, C-SO_2-C, and SO_x groups along the entire inner, and outer surfaces (see XPS-,

Raman shift and EDX-SEM mapping- analysis). The functional S-active sites and groups induce the negative charge and increase the spine density at the outer surface, as evidenced from Zeta potential plot (Figure S2C). On the other hand, the NEP acid-base behavior in reaction media leads to the formation of protonated H_3NEP^+, neutral H_2NEP, and anion $HNEP^-$ groups. At physiological pH (pH = 7.4) condition, the H_3NEP^+ constituents (at pKa = 8.64) are dominant, while the chance for the presence of anion form is negligibly considered.[58]

This finding indicates the formation of positively charged NEP in the solution. Therefore, the S-CNS-to-NEP interaction at the electrode surface would be strong due to the electrostatic binding between NEP-molecules and functional S-active sites and groups. The current peak intensity depends on the adsorbed NEP on the S-CSN-1 electrode surface. The total adsorbed NEP amount on the S-CSN-1 electrode surface was estimated by applying the Randles–Sevcik equation:[59]

$$I_p = n - 2F2\Gamma\nu A/4RT, \quad (1)$$

where A is the bare GCE surface area, n is the number of electrons transferred, ν is the scan rate, F is the Faraday constant, T is the absolute temperature, R is the gas constant, and Γ is the total concentration of NEP on the S-CSN-1 electrode surface. The calculated Γ equals 27.2 $\times 10^{-6}$ mole/cm^2.

The charge transfer coefficient (α) and electron transfer rate constant (Ks) of the NEP redox reaction on the S-CSN-1-modified electrode surface can be obtained based on the relation of log ν versus the applied potential (E), within the scan rate range of 10–100 mVs^{-1}. The linear relationship of log ν Vs E (V) was obtained with regression equations of Ea(V) = 0.306 + 0.009 log ν (V s^{-1}) (R^2 = 0.84) and Ec(V) = 0.326 - 0.012 log ν (V s^{-1}) (R^2 = 0.87). By applying Laviron's theory, [60]

$$\log k_a/k_c = \log \alpha/(1-\alpha) \text{ or } (k_a)/k_c = \alpha/(1-\alpha) \quad (2)$$

where Ka is the slope of Ea versus log ν and equal to 2.3RT/(1 − α)nF, and Kc (the slope of Ec vs log ν) is −2.3RT/αnF. Charge transfer coefficient (α) was calculated to be 0.3 s.

The heterogeneous electron transfer rate constant (K_s) can be calculated (Laviron 1979) by applying this equation:

$$\log k_s = \alpha \log(1-\alpha) + (1-\alpha)\log\alpha - \log\frac{RT}{nFv} - \frac{\alpha(1-\alpha)nF\Delta E_p}{2.3RT} \qquad (3)$$

where α is the charge transfer coefficient, n is the number of electrons evolved in the reaction, ν is the scan rate, and ΔEp is the anodic and cathodic peak separation potential. The K_s value is 0.25 cms^{-1}. Therefore, the S-CSN-1-modified electrode exhibits efficient and high charge transfer between the electrolyte electrode interfaces. The nanosensor with topographical and morphological construction of 3D curvature, meso-grooves, ridge end, rugged surface texture, S-doped the carbon chain led to the formation of a highly active surface with facile molecular/electron diffusion, multi-diffusive centers, and high loading of NEP molecules.

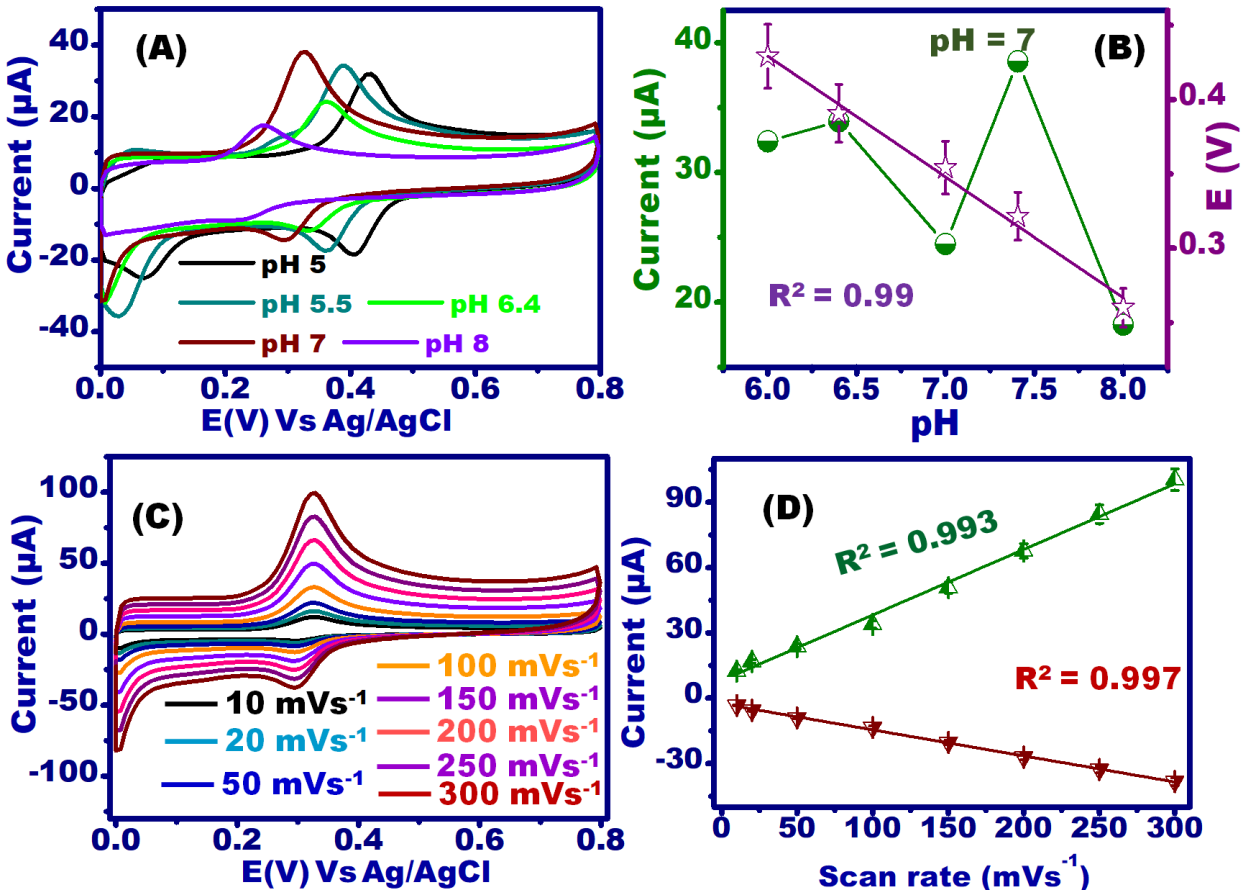

Figure 3. A) CVs of pH-dependent monitoring assay of 20 µM NEP using S-CSN-1-modified electrode at various pH-values ranging from 5 to 8 at scan rate of 100 mVs^{-1}, under N_2 saturation. B) Linear-, and scatter- plots of the pH-values versus the anodic current (µA) (green scatter) and applied potential (E/V) (violet points). C) CVs of 20 µM NEP under various scan rates of 10-300 mVs^{-1} in 0.1 M PBS (pH = 7) on S-CSN-1-modified electrode, and B) plot of scan rate (mVs^{-1}) vs corresponding anodic (I_a) and cathodic (I_c) currents (µA).

3.4 Sensitivity, selectivity, stability, and reproducibility of the S-CSN-1-modified electrode

The sensitive approach and the calibration curve of the S-CSN-1-modified electrode were determined using square wave voltammetry (SWV). The SWV electrochemical technique enabled the precision determination of NEP sensitivity at ultra-trace concentration. Figure 4A shows the SWV-measurements of various concentration of NEP from 0.01 to 100 μM (0.1 M PBS, pH = 7) by using the S-CSN-1-modified electrode. The sensitive current response was observed upon adding and increasing the concentrations of NEP. Figure 4B shows the calibration plot of NEP concentrations (μM) versus the current (μA) within the range of 0.01– 0.8 μM. A linear relationship was obtained with following the equation of I (μA) = 0.76 + 11.54 [NEP](μM), R^2 = 0.989 (S/N = 3). The limit of detection is 0.001 μM, with a wide linear range of 0.01–0.8 μM. The linearity was distorted at high concentrations of NEP possibly due to electrode saturation (Figure 4C). These results provide a highly sensitive protocol for signaling of NEP at ultra-trace levels with a wide linear range by using the S-CSN-1-modified electrode. S-CSN-1 provides highly sensitive detection of NEP with low detection limits and a wide linear range and thus could be a sensitive biosensor for clinical applications. The high sensitivity with a wide linear range of S-CSN-1 may relate to the morphology of spherical surface with rough contact surface, open carbon network of S dopant atoms, active functionalization of the active interfacial surface, high surface area, and microporous construction. Moreover, NEP molecules diffuse through the pores and binds strongly to the S-CSN-1 active sites, resulting in multi-diffusive electrode surface with fast charge transport.

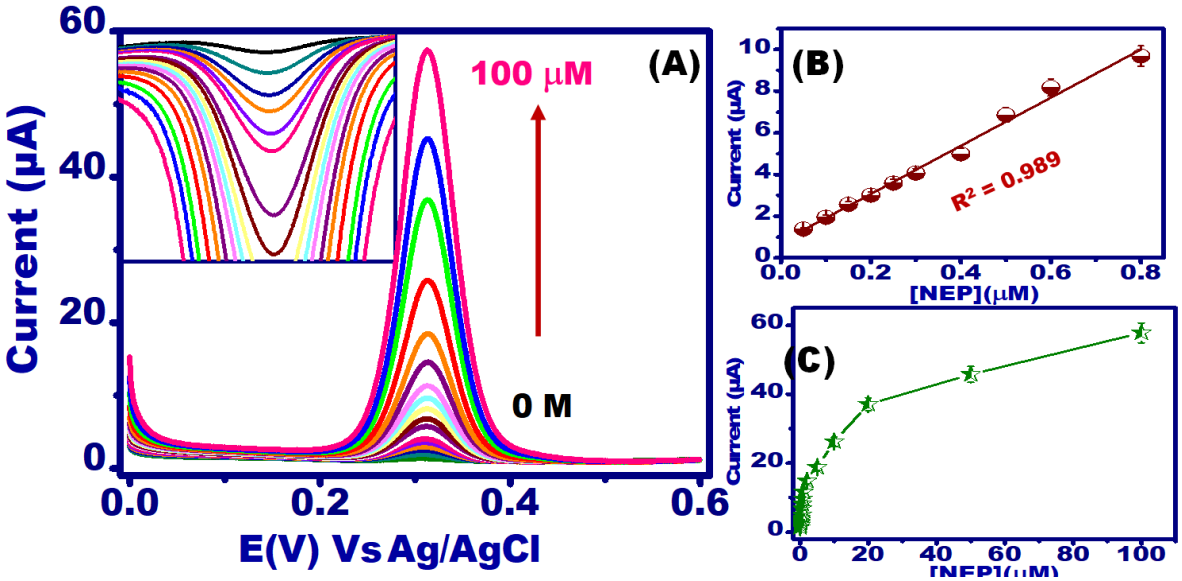

Figure 4. A) SWV-measurements of the S-CSN-1-modified electrode at various concentrations of NEP (0.01-100 µM) were performed, its inset shows the SWV at low concentrations. B) Calibration plot of [NEP] (µM) (0.01 – 0.8) versus the current (µA). C) The plot of the whole concentration range of NEP (0.01 – 100 µM) versus the current (µA).

Electrode selectivity was studied as a function of potential interfering molecules such as ascorbic acid (AA), DA, EP, and uric acid (UA). These biomolecules are usually present in human body fluids and overlap with the NEP-oxidation peak. Figure S3 shows the column plot of NEP concentration and the concentrations of AA, UA, DA, and EPI. Meanwhile, no response of AA, UA is observed at the same detection level of NEP, while a small interfering effect is notified for DA, and EPI. These results provide highly selective biosensor for signaling NEP. The designed biosensor of S-CSN-1 showed the lowest detection limit compared with the other modified electrodes of various sensors (Table S1). In the view of electrode applicability, the low-cost fabrication and excellent features of the portable neurotransmitter senor electrode are of interest.

In this regard, the S-CNS electrode was prepared by simple approach, low-cost material source, and sensitive behavior without needs of any treatment with strong acid/alkaline solutions. In addition, the S-CNS electrode is highly stable structural property (see Figure S4A). FE-SEM patterns show the structure stability of reusable S-CNS electrode after 200 cycles, despite the electro-polymerization of NEP at the electrode surface. Furthermore, the designed biosensor of S-CSN-1 showed high stability and good reproducibility, with RSD of 1.7 up to 5 samples and 5 electrodes [for additional details see supporting information, Figure S4 (B&C)].

3.7 Selective signaling of NEP in human blood serum and secreted from PC12 cells under-stimulation agent

The validity of the biosensor for real monitoring of NEP in human fluids, such as human blood serum, was determined. Various concentrations of NEP were spiked in 0.1 M PBS (pH= 7) holding 10 μL of human serum and measured by SWV technique (S/N = 3). Table S2 shows the recovery of NEP on the S-CSN-modified electrode. The high recovery of the spiked samples was obtained, ranging from 98% to 99.9%. These results confirm the suitability of the S-CSN-1-modified electrode for detection of NEP in human serum samples and can be employed for clinical application due to its fast response, high sensitivity, good selectivity, and promising economical value.

Successful detection of the levels of monoamine neurotransmitters (i.e., NEP) in the samples of human tissues (neuronal cells, and in the brain) is highly needed for investigation of some neurological diseases, such as schizophrenia. PC12 cells acted as the model of the nervous system cells. In vitro monitoring of NEP liberated from neuronal cells, such as PC12, was evaluated under various concentrations of stimulating agents, such as KCl solution. First, designing sensitive and

selective materials with high biocompatibility open the chance for cellular sensing application. Thus, a laser scanning confocal microscopy of S-CSN within the cells after incubation for 4 h was conducted (Figure 5A-D). S-CSN and cells were evaluated by bright-field images. S-CSN surrounded the cell membrane of PC12 (Figure 5A). Moreover, the cells were stained by phalloidin for F-actin counterstaining and the nucleus was stained by DAPI. The merged image of the cells confirmed the S-CSN biocompatibility, as presented in Figure 5 B-D. The cell's cytoplasm and nucleus are not affected by S-CSN and shrinkage on the cell membrane and change in the cell's nucleus were not observed. These data confirm the high biocompatibility of S-CSN when incubated with PC12 cells. Therefore, S-CSN exhibits potential for further in vitro and in vivo studies.

The cytotoxicity of the materials was further confirmed. The cells were grown in 96 well-plate with a concentration of 4×10^5 cells/mL. Various concentrations of S-CSN (10-200 µg/mL) were incubated with the cells for 24 h by using Cell Counting Kit-8 (CCK-8) assays and measured by a microplate reader. Figure 5E shows the scatter of the concentrations of the materials versus cell viability. The plot configures the significant low cytotoxicity of S-CSN. The cells lose only 23% of its viability at a high concentration of 200 µg/mL and lost only less than 7% at 10 µg/mL. Thus, S-CSN exhibits low cytotoxicity and high biocompatibility within the living cells and has high applicability for monitoring NEP in living cells.

The in vitro monitoring and setting up of NEP biosensor protocol were performed using SWV under the optima conditions. The NEP secreted from PC12 cell was measured by taking the supernatants of 3×10^6 cells/mL PC12 and determined using the S-CSN-modified electrode. The PC12 cells were incubated with various concentrations of stimulating agents (0 – 50 mM KCl) for 30 min. Figure 5F shows the plot of KCl concentration (mM) versus the current (µA). To confirm

the sensitive detection of NEP using the S-CNS-1-modified electrode, the specific concentration of NEP secreted from PC12 ($2x10^6$ cells/mL) was confirmed by CV measurements. Figure 5G shows the CVs of various cells supernatant that incubated with various concentrations of KCl (10 – 50 mM) for 30 min. The column plot of KCl concentrations (mM) versus the responded current (μA) indicates the sensitive and selective detection of NEP secreted from living cells under K^+–stimulation (Figure 5H). The extracellular NEP was stimulated under the presence of K^+ ions. The key role of K^+-ions was determined by depolarization of the cell membrane and induction of the influx of Ca^{2+} and Na^+ to open the voltage-sensitive Na^+ and Ca^{2+} channels. [4, 8, 61-62] The anodic current of NEP molecules secreted from the neuronal cell line model of PC12 depends on K^+ concentration. Therefore, the designed biosensor of S-CSN can selectively and sensitively detect NEP in living cells. Moreover, the designed biosensor of S-CSN can be employed for clinical application and early diagnosis of some neuronal diseases, such as schizophrenia. The proposed sensing protocol exhibits high sensitivity, selectivity, low cytotoxicity, and high biocompatibility.

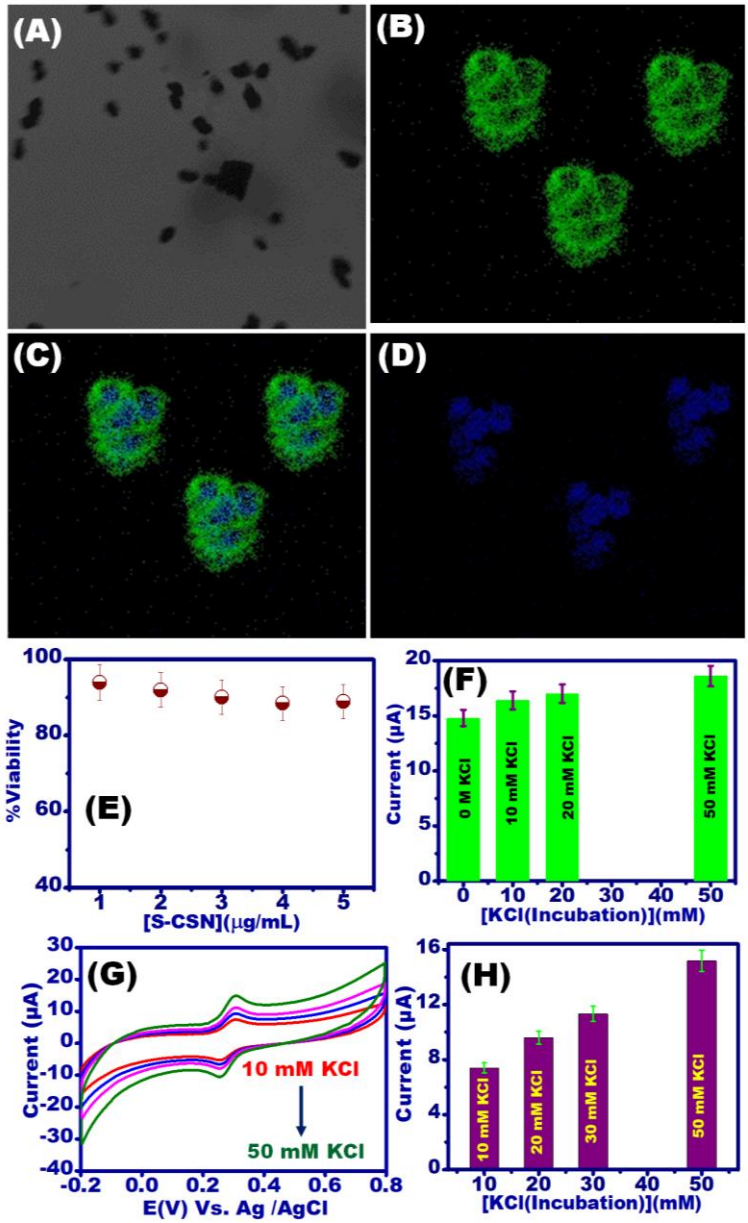

Figure 5. (A-D) Confocal microscopy images recorded at an excitation wavelength of 405, and 488 nm DAPI, and phalloidin. A) Bright-field image of S-CSN-1 incubated with PC12 cells. B) Filamentous actin staining (phalloidin) of PC12 image. C) Merged image of nucleus and f-actin of PC12 upon incubation with S-CSN-1. D) Nucleus counter staining (DAPI) of PC12 cells image. F) Cytotoxicity assay of S-CSN-1 on the PC12 cell line with various concentrations (10 – 200 μg/mL) using a CCK-8 assay protocol and measured by a microplate reader at 450 nm. F) The

column plot of the [K^+]/mM versus the secreted NEP from the PC12 cells ($3x10^6$ cells/mL) using SWV-measurements in the range of 0 – 50 mM. G) CVs of cells supernatant incubated with various concentrations of KCl (10 –50 mM). F) The column plot of the [K^+]/mM versus the secreted NEP from the PC12 cells ($2x10^6$ cells/mL) using CV-measurements in the range of 10–50 mM.

4. Conclusion

This work developed NEP biosensor based on a metal-free electrode of 3D-circular surface curvature of spherule surface (S-CSN) that has high sensitivity and selectivity, fast response, and biocompatibility. S-CSN was designed based on the controlled spheroidal nanolayer formation. The 3D-circular surface curvature of spherule-based electrode was successfully fabricated from stacked layer-by-layer approach that orientated around one axis to form ellipsoid structure morphologies. The designed electrode surface showed 3D curvature surface, rough surface texture with ridge ends, and bundle surface meshes. The surface topography and morphology of S-CSN carried over the outer surface coverage of electrodes into tightly folded sensor surfaces. The S-CSN-based biosensor established a highly active interfacial surface for selective detection of NEP with fast electron transfer, long and circular molecular diffusion, low charge distance pathway, and strong binding to NEP molecules. S-CSN-1 provides a sensitive sensing protocol with high stability, good reproducibility, a low detection limit of 0.001 μM, and a wide linear range of 0.01–0.8 μM. The real monitoring of NEP in human blood serum with high recovery of up to 99.9% set up a readable sample based on the S-CSN-1-modified electrode. The sensing protocol could be an in vitro assay for signaling NEP from living cells. S-CSN-1 provides highly sensitive and selective

biosensor for signaling NEP in its resources and receptors with low cytotoxicity and high biocompatibility for clinical investigation of several neuronal diseases.

ASSOCIATED CONTENT

Supporting Information

Supporting information included materials and methods, chemical reagents, electrochemical sensing system, and characterization analysis, XPS analysis of S-CNS, catalytic activity of S-CNS-1 and S-CNS-2, and stability and reproducibility studies.

AUTHOR INFORMATION

Corresponding Author

National Institute for Materials Science (NIMS), Research Center for Functional Materials, 1-2-1 Sengen, Tsukuba-shi, Ibaraki-ken 305-0047, Japan

** Corresponding author: sherif.elsafty@nims.go.jp*

Funding Sources

This work was supported by the Japan Society for the Promotion of Science (JSPS), grant No. P19067.

ACKNOWLEDGMENT

We thank Dr Miwako Takano, Young International Research Center (ICYS), NIMS for assistance.

REFERENCES

(1) Casadio, S.; Lowdon, J.; Betlem, K.; Ueta, J.; Foster, C. W.; Cleij, T.; van Grinsven, B.; Sutcliffe, O.; Banks, C. E.; Peeters, M. Development of a novel flexible polymer-based biosensor platform for the thermal detection of noradrenaline in aqueous solutions. *Chem. Eng. J.***2017,** *315*, 459-468.

(2) Moghzi, F.; Soleimannejad, J.; Sañudo, E. C.; Janczak, J. Dopamine sensing based on ultrathin fluorescent metal-organic nanosheets. *ACS Appl.Mater. Interfaces* **2020**. https://doi.org/10.1021/acsami.0c13166

(3) Emran, M. Y.; Mekawy, M.; Akhtar, N.; Shenashen, M. A.; EL-Sewify, I. M.; Faheem, A.; El-Safty, S. A. Broccoli-shaped biosensor hierarchy for electrochemical screening of noradrenaline in living cells. *Biosens.Bioelectron.* **2018,** *100*, 122-131.

(4) Emran, M. Y.; Shenashen, M. A.; Morita, H.; El-Safty, S. A. 3D-Ridge Stocked Layers of Nitrogen-Doped Mesoporous Carbon Nanosheets for Ultrasensitive Monitoring of Dopamine Released from PC12 Cells under K+ Stimulation. *Adv. Halthcare Mater.* **2018**, 1701459.

(5) Eisenhofer, G.; Pacak, K.; Huynh, T.-T.; Qin, N.; Bratslavsky, G.; Linehan, W. M.; Mannelli, M.; Friberg, P.; Timmers, H. J.; Bornstein, S. R. Catecholamine metabolomic and secretory phenotypes in phaeochromocytoma. *Endocrine-related cancer* **2011,** *18* (1), 97.

(6) Bravo, E. L.; Tagle, R. Pheochromocytoma: state-of-the-art and future prospects. *Endocrine Rev.* **2003,** *24* (4), 539-553.

(7) Terbeck, S.; Savulescu, J.; Chesterman, L.; Cowen, P. Noradrenaline effects on social behaviour, intergroup relations, and moral decisions. *Neurosc.Biobehavioral Rev.***2016,** *66*, 54-60.

(8) Emran, M. Y.; Shenashen, M. A.; Morita, H.; El-Safty, S. A. One-step selective screening of bioactive molecules in living cells using sulfur-doped microporous carbon. *Biosens.Bioelectron.* **2018,** 109, 237-245.

(9) Cova, I.; Priori, A. Diagnostic biomarkers for Parkinson's disease at a glance: where are we? *J.Neural Transm.* **2018,** *125* (10), 1417-1432.

(10) Cerroni, R.; Liguori, C.; Stefani, A.; Conti, M.; Garasto, E.; Pierantozzi, M.; Mercuri, N. B.; Bernardini, S.; Fucci, G.; Massoud, R. Increased Noradrenaline as an Additional Cerebrospinal Fluid Biomarker in PSP-Like Parkinsonism. *Front. Aging Neurosc.* **2020,** *12*, 126.

(11) Emran, M. Y.; Shenashen, M. A.; Mekawy, M.; Azzam, A. M.; Akhtar, N.; Gomaa, H.; Selim, M. M.; Faheem, A.; El-Safty, S. A. Ultrasensitive in-vitro monitoring of monoamine neurotransmitters from dopaminergic cells. *Sens.Actuators B: Chem.* **2018,** *259*, 114-124.

(12) Reinhoud, N. J.; Brouwer, H.-J.; van Heerwaarden, L. M.; Korte-Bouws, G. A. Analysis of glutamate, GABA, noradrenaline, dopamine, serotonin, and metabolites using microbore UHPLC with electrochemical detection. *ACS Chem. Neurosc.* **2013,** *4* (5), 888-894.

(13) Zhou, Q.; Kang, S.-Z.; Li, X.; Wang, L.; Qin, L.; Mu, J. One-pot hydrothermal preparation of wurtzite CuGaS2 and its application as a photoluminescent probe for trace detection of l-noradrenaline. *Coll. Surfaces A: Physicochem. Eng. Aspects* **2015,** *465*, 124-129.

(14) Robert, F.; Bert, L.; Lambás-Señas, L.; Denoroy, L.; Renaud, B. In vivo monitoring of extracellular noradrenaline and glutamate from rat brain cortex with 2-min microdialysis sampling using capillary electrophoresis with laser-induced fluorescence detection. *J. Neurosc. Meth.* **1996,** *70* (2), 153-162.

(15) Amiri-Aref, M.; Raoof, J. B.; Ojani, R. A highly sensitive electrochemical sensor for simultaneous voltammetric determination of noradrenaline, acetaminophen, xanthine and

caffeine based on a flavonoid nanostructured modified glassy carbon electrode. *Sens. Actuators B: Chem.* **2014,** *192*, 634-641.

(16) Devnani, H.; Satsangee, S. P.; Jain, R. Nanocomposite modified electrochemical sensor for sensitive and selective determination of noradrenaline. *Mater. Today: Proceed.* **2016,** *3* (6), 1854-1863.

(17) Akhtar, N.; Emran, M. Y.; Shenashen, M. A.; Khalifa, H.; Osaka, T.; Faheem, A.; Homma, T.; Kawarada, H.; El-Safty, S. A. Fabrication of photo-electrochemical biosensors for ultrasensitive screening of mono-bioactive molecules: the effect of geometrical structures and crystal surfaces. *J. Mater. Chem. B* **2017,** *5* (39), 7985-7996.

(18) Abdelwahab, A. A.; Naggar, A. H.; Abdelmotaleb, M.; Emran, M. Y. Ruthenium Nanoparticles Uniformly-designed Chemically Treated Graphene Oxide Nanosheets for Simultaneous Voltammetric Determination of Dopamine and Acetaminophen. *Electroanalysis* **2020**. https://doi.org/10.1002/elan.202060126

(19) Taei, M.; Jamshidi, M. S. A voltammetric sensor for simultaneous determination of ascorbic acid, noradrenaline, acetaminophen and tryptophan. *Microchem. J.* **2017,** *130*, 108-115.

(20) Beitollahi, H.; Mohammadi, S. Selective voltammetric determination of norepinephrine in the presence of acetaminophen and tryptophan on the surface of a modified carbon nanotube paste electrode. *Mater. Sci. Eng. C* **2013,** *33* (6), 3214-3219.

(21) Pahlavan, A.; Gupta, V. K.; Sanati, A. L.; Karimi, F.; Yoosefian, M.; Ghadami, M. ZnO/CNTs nanocomposite/ionic liquid carbon paste electrode for determination of noradrenaline in human samples. *Electrochim. Acta* **2014,** *123*, 456-462.

(22) Siuzdak, K.; Ficek, M.; Sobaszek, M.; Ryl, J.; Gnyba, M.; Niedziałkowski, P.; Malinowska, N.; Karczewski, J.; Bogdanowicz, R. Boron-enhanced growth of micron-scale carbon-based

nanowalls: a route toward high rates of electrochemical biosensing. *ACS Appl.Mater. Interfaces* **2017,** *9* (15), 12982-12992.

(23) Cha, C.; Shin, S. R.; Annabi, N.; Dokmeci, M. R.; Khademhosseini, A. Carbon-based nanomaterials: multifunctional materials for biomedical engineering. *ACS Nano* **2013,** *7* (4), 2891-2897.

(24) Emran, M. Y.; Shenashen, M. A.; Abdelwahab, A. A.; Abdelmottaleb, M.; El-Safty, S. A. Facile synthesis of microporous sulfur-doped carbon spheres as electrodes for ultrasensitive detection of ascorbic acid in food and pharmaceutical products. *New J. Chem.* **2018,** *42* (7), 5037-5044.

(25) Lu, C.; Liu, Y.; Ying, Y.; Liu, J. Comparison of MoS2, WS2, and graphene oxide for DNA adsorption and sensing. *Langmuir* **2017,** *33* (2), 630-637.

(26) Raphey, V.; Henna, T.; Nivitha, K.; Mufeedha, P.; Sabu, C.; Pramod, K. Advanced biomedical applications of carbon nanotube. *Mater. Sci. Eng. C* **2019,** 100, 616 - 630.

(27) Alim, S.; Vejayan, J.; Yusoff, M. M.; Kafi, A. Recent uses of carbon nanotubes & gold nanoparticles in electrochemistry with application in biosensing: A review. *Biosens. Bioelectron.* **2018,** 121, 125 - 136.

(28) Shenashen, M. A.; Hassen, D.; El-Safty, S. A.; Isago, H.; Elmarakbi, A.; Yamaguchi, H. Axially oriented tubercle vein and X-crossed sheet of N-Co3O4@ C hierarchical mesoarchitectures as potential heterogeneous catalysts for methanol oxidation reaction. *Chem. Eng. J.* **2017,** *313*, 83-98.

(29) Ding, X.; Bai, J.; Xu, T.; Li, C.; Zhang, H.-M.; Qu, L. A novel nitrogen-doped graphene fiber microelectrode with ultrahigh sensitivity for the detection of dopamine. *Electrochem.Commun.* **2016,** *72*, 122-125.

(30) Fan, S.; Zhao, M.; Ding, L.; Liang, J.; Chen, J.; Li, Y.; Chen, S. Synthesis of 3D hierarchical porous Co3O4 film by eggshell membrane for non-enzymatic glucose detection. *J. Electroanal. Chem.* **2016,** *775*, 52-57.

(31) Khalifa, H.; El-Safty, S. A.; Reda, A.; Shenashen, M. A.; Selim, M. M.; Elmarakbi, A.; Metawa, H. A. Theoretical and Experimental Sets of Choice Anode/Cathode Architectonics for High-Performance Full-Scale LIB Built-up Models. *Nano-Micro Lett.* **2019,** *11* (1), 84.

(32) Khalifa, H.; El-Safty, S. A.; Reda, A.; Shenashen, M. A.; Elmarakbi, A.; Metawa, H. A. Structurally Folded Curvature Surface Models of Geodes/Agate Rosettes (Cathode/Anode) as Vehicle/Truck Storage for High Energy Density Lithium-Ion Batteries. *Batteries & Supercaps* **2020,** *3* (1), 76-92.

(33) Khalifa, H.; Shenashen, M. A.; Reda, A.; Selim, M. M.; Elmarakb, A.; El-Safty, S. A. Complex Structure Model Mutated Anode/Cathode Electrodes for Improving Large-Scale Battery Designs. *ACS Appl. Energy Mater.***2020,** *3* (9), 9168-9181.

(34) Gomaa, H.; Khalifa, H.; Selim, M.; Shenashen, M.A.; Kawada, S.; Alamoudi, A. S.; Azzam, A.; Alhamid, A.; El-Safty, S. Selective, photoenhanced trapping/detrapping of arsenate anions using mesoporous blobfish head TiO2 monoliths. *ACS Sus. Chem. Eng.* **2017,** *5* (11), 10826-10839.

(35) Gomaa, H.; Shenashen, M.A.; Yamaguchi, H.; Alamoudi, A.; El-Safty, S. Extraction and recovery of Co 2+ ions from spent lithium-ion batteries using hierarchical mesosponge γ-Al 2 O 3 monolith extractors. *Green Chem.* **2018,** *20* (8), 1841-1857.

(36) Shenashen, M. A.; Hassen, D.; El-Safty, S. A.; Selim, M. M.; Akhtar, N.; Chatterjee, A.; Elmarakbi, A. Mesoscopic Fabric Sheet Racks and Blocks as Catalysts with Efficiently

Exposed Surfaces for Methanol and Ethanol Electrooxidation. *Adv. Mater. Interfaces* **2016,** *3* (24), 1600743,.

(37) Li, J.; Jiang, J.; Feng, H.; Xu, Z.; Tang, S.; Deng, P.; Qian, D. Facile synthesis of 3D porous nitrogen-doped graphene as an efficient electrocatalyst for adenine sensing. *RSC Adv.* **2016,** *6* (37), 31565-31573.

(38) Li, R.; Wei, Z.; Gou, X.; Xu, W. Phosphorus-doped graphene nanosheets as efficient metal-free oxygen reduction electrocatalysts. *RSc Adv.* **2013,** *3* (25), 9978-9984.

(39) Sheng, Q.; Liu, R.; Zheng, J. Fullerene–nitrogen doped carbon nanotubes for the direct electrochemistry of hemoglobin and its application in biosensing. *Bioelectrochem.* **2013,** *94*, 39-46.

(40) Sheng, Z.-H.; Gao, H.-L.; Bao, W.-J.; Wang, F.-B.; Xia, X.-H. Synthesis of boron doped graphene for oxygen reduction reaction in fuel cells. *J. Mater. Chem.* **2012,** *22* (2), 390-395.

(41) Jeon, I. Y.; Zhang, S.; Zhang, L.; Choi, H. J.; Seo, J. M.; Xia, Z.; Dai, L.; Baek, J. B. Edge-selectively sulfurized graphene nanoplatelets as efficient metal-free electrocatalysts for oxygen reduction reaction: the electron spin effect. *Adv. Mater.* **2013,** *25* (42), 6138-6145.

(42) Huang, B.; Hu, X.; Liu, Y.; Qi, W.; Xie, Z. Biomolecule-derived N/S co-doped CNT-graphene hybrids exhibiting excellent electrochemical activities. *J. Power Sour.* **2019,** *413*, 408-417.

(43) Wang, Q.; Li, H.; Chen, L.; Huang, X. Novel spherical microporous carbon as anode material for Li-ion batteries. *Solid State Ionics* **2002,** *152*, 43-50.

(44) El-Safty, S.; Shenashen, M.; Ismael, M.; Khairy, M. Mesocylindrical Aluminosilica Monolith Biocaptors for Size-Selective Macromolecule Cargos. *Adv.Functional Mater.* **2012,** *22* (14), 3013-3021.

(45) El-Safty, S. A.; Sakai, M.; Selim, M. M.; Hendi, A. A. Mesosponge optical sinks for multifunctional mercury ion assessment and recovery from water sources. *ACS Appl. Mater. & Interfaces* **2015,** *7* (24), 13217-13231.

(46) Elshehy, E. A.; EL-Safty, S. A.; Shenashen, M. A. Reproducible design for the optical screening and sensing of Hg (II) ions. *Chemosensors* **2014,** *2* (4), 219-234.

(47) Khairy, M.; El-Safty, S. A. Promising supercapacitor electrodes based immobilization of proteins onto macroporous Ni foam materials. *J. Energy Chem.* **2015,** *24* (1), 31-38.

(48) Sun, Y.; Wu, J.; Tian, J.; Jin, C.; Yang, R. Sulfur-doped carbon spheres as efficient metal-free electrocatalysts for oxygen reduction reaction. *Electrochim. Acta* **2015,** *178*, 806-812.

(49) Kim, H. T.; Shin, H.; Jeon, I. Y.; Yousaf, M.; Baik, J.; Cheong, H. W.; Park, N.; Baek, J. B.; Kwon, T. H. Carbon–Heteroatom Bond Formation by an Ultrasonic Chemical Reaction for Energy Storage Systems. *Adv. Mater.* **2017,** *29* (47), 1702747.

(50) Buttry, D.; Bard, A., Electroanalytical chemistry, vol. 17. New York: Marcel Dekker: 1991.

(51) Akhtar, N.; El-Safty, S. A.; Abdelsalam, M. E.; Kawarada, H. One-pot fabrication of dendritic NiO@ carbon–nitrogen dot electrodes for screening blood glucose level in diabetes. *Adv. Healthcare Mater.* **2015,** *4* (14), 2110-2119.

(52) Akhtar, N.; El-Safty, S. A.; Abdelsalam, M. E.; Shenashen, M. A.; Kawarada, H. Radially oriented nanostrand electrodes to boost glucose sensing in mammalian blood. *Biosens. Bioelectron.* **2016,** *77*, 656-665.

(53) Emran, M. Y.; El-Safty, S. A.; Shenashen, M. A.; Minowa, T. A well-thought-out sensory protocol for screening of oxygen reactive species released from cancer cells. *Sens. Actuators B: Chem.* **2018**.

(54) Emran, M. Y.; Khalifa, H.; Gomaa, H.; Shenashen, M. A.; Akhtar, N.; Mekawy, M.; Faheem, A.; El-Safty, S. A. Hierarchical CN doped NiO with dual-head echinop flowers for ultrasensitive monitoring of epinephrine in human blood serum. *Microchim. Acta* **2017,** *184* (11), 4553-4562.

(55) Li, Y.; Gu, Y.; Zheng, B.; Luo, L.; Li, C.; Yan, X.; Zhang, T.; Lu, N.; Zhang, Z. A novel electrochemical biomimetic sensor based on poly (Cu-AMT) with reduced graphene oxide for ultrasensitive detection of dopamine. *Talanta* **2017,** *162*, 80-89.

(56) Emran, M. Y.; Shenashen, M. A.; Abdelwahab, A. A.; Abdelmottaleb, M.; Khairy, M.; El-Safty, S. A. Nanohexagonal Fe 2 O 3 electrode for one-step selective monitoring of dopamine and uric acid in biological samples. *Electrocatalysis* **2018,** *9* (4), 514-525.

(57) Emran, M. Y.; Shenashen, M. A.; Abdelwahab, A. A.; Khalifa, H.; Mekawy, M.; Akhtar, N.; Abdelmottaleb, M.; El-Safty, S. A. Design of hierarchical electrocatalytic mediator for one step, selective screening of biomolecules in biological fluid samples. *J. Appl.Electrochem.* **2018,** *48* (5), 529-542.

(58) Álvarez-Diduk, R. n.; Galano, A. Adrenaline and noradrenaline: protectors against oxidative stress or molecular targets? *J. Phys. Chem. B* **2015,** *119* (8), 3479-3491.

(59) Bard, A. J. LR Faulkner electrochemical methods. *W iley, New York* **1980**.

(60) Laviron, E. General expression of the linear potential sweep voltammogram in the case of diffusionless electrochemical systems. *J. Electroanal. Chem. Interfacial Electrochem.* **1979,** *101* (1), 19-28.

(61) Shinohara, H.; Sakai, Y.; Mir, T. A. Real-time monitoring of intracellular signal transduction in PC12 cells by two-dimensional surface plasmon resonance imager. *Anal. Biochem.* **2013,** *441* (2), 185-189.

(62) Mir, T. A.; Akhtar, M. H.; Gurudatt, N.; Kim, J.-I.; Choi, C. S.; Shim, Y.-B. An amperometric nanobiosensor for the selective detection of K+-induced dopamine released from living cells. *Biosen. Bioelectron.* **2015,** *68*, 421-428.

Graphical abstract

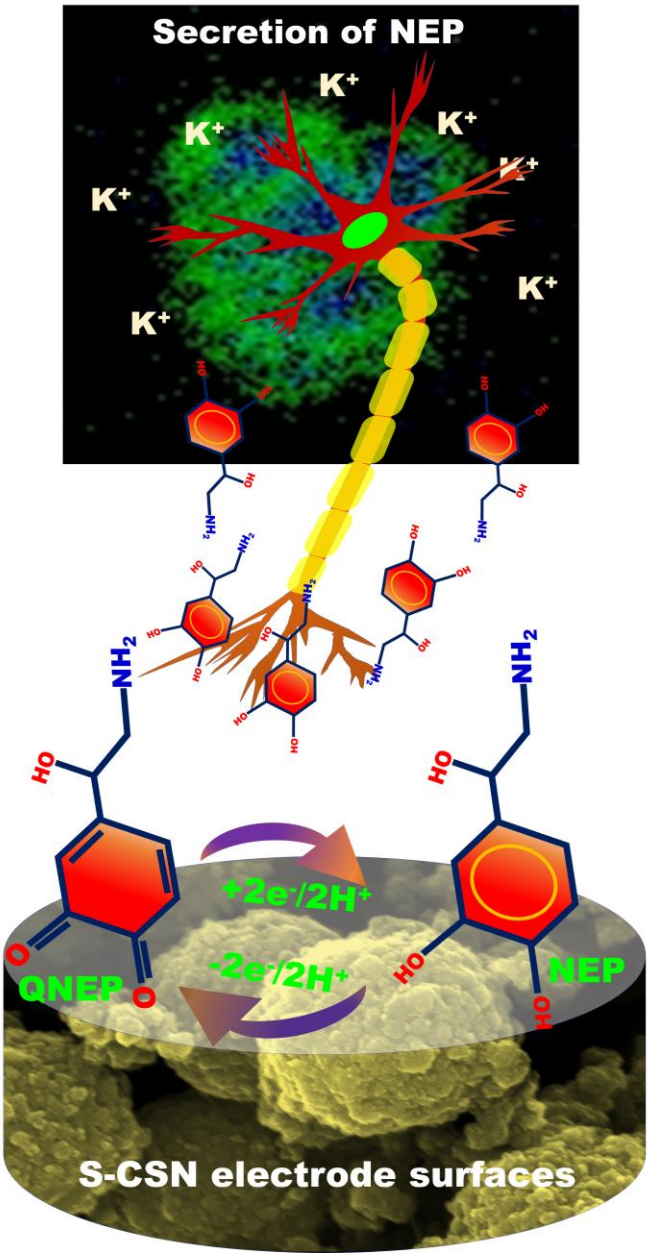

Highly active biosensor design based on S-doped carbon spheroidal surface (S-CSN) for ultrasensitive monitoring of norepinephrine secreted from living cells (PC12). The S-CSN shows sensitive and selective nanosensor for in-vitro monitoring of NEP with high biocompatibility, low cytotoxicity, high stability, and good reproducibility.